Draft version November 4, 2026
Typeset using LaTeX **twocolumn** style in AASTeX7

arXiv:2611.03801v1 [astro-ph.GA] 2 Nov 2026

# Ly$\alpha$ in Compact Broad-Line Emitters, Including Little Red Dots, Is More Closely Linked to the Host Galaxy than to the Broad-Line Nucleus

Yongda Zhu [1,*] Zheng Ma [1,*] Xiaojing Lin [2] Junyu Zhang [1] Jianwei Lyu [1] Xiaohui Fan [1] Eiichi Egami [1] Andrew J. Bunker [3] Sijia Cai [2] Laura C. Keating [4] Joseph Shields [5] Zhiyuan Ji [1] Xiangyu Jin [6] Weizhe Liu [1] Suprabhas Narisetty [7] George H. Rieke [1] Marcia J. Rieke [1] Pierluigi Rinaldi [8] and Fengwu Sun [9,10]

[1] *Steward Observatory, University of Arizona, 933 North Cherry Avenue, Tucson, AZ 85721, USA*
[2] *Department of Astronomy, Tsinghua University, Beijing 100084, China*
[3] *Department of Physics, University of Oxford, Denys Wilkinson Building, Keble Road, Oxford OX1 3RH, UK*
[4] *Institute for Astronomy, University of Edinburgh, Blackford Hill, Edinburgh, EH9 3HJ, UK*
[5] *Large Binocular Telescope Observatory, Tucson, AZ, USA*
[6] *Department of Astronomy, University of Michigan, 1085 S. University Ave., Ann Arbor, MI 48109, USA*
[7] *Department of Astronomy, University of Illinois Urbana-Champaign, 1002 W. Green Street, Urbana, IL 61801, USA*
[8] *Space Telescope Science Institute, 3700 San Martin Drive, Baltimore, Maryland 21218, USA*
[9] *Department of Astronomy, Westlake University, Hangzhou 310030, Zhejiang Province, China*
[10] *Center for Astrophysics | Harvard & Smithsonian, 60 Garden St., Cambridge, MA 02138, USA*

## ABSTRACT

JWST has found many faint broad-line AGN at $z > 4$, but it is unclear whether the Ly$\alpha$ we see from them comes from the accreting black hole or from its host galaxy. The answer matters for how these sources are interpreted and for how many ionizing photons they release. We use deep JWST/NIRSpec spectroscopy from the DIVER program to measure Ly$\alpha$ in 12 compact broad-line emitters (CBEs) at $z = 4.2$–$5.5$ in GOODS-N. CBEs include little red dots (LRDs), little blue dots, and other broad-line AGN. Six are detected in Ly$\alpha$. Every source shows a broad-line region, yet Ly$\alpha$ does not follow it: the sources with the strongest H$\alpha$ relative to the UV include weak detections and nondetections, and every detected Ly$\alpha$ line (FWHM $\approx$ 300–1000 km s$^{-1}$) is narrower than broad H$\alpha$ (1100–3300 km s$^{-1}$). Instead, Ly$\alpha$ appears to track the host galaxy. We model the AGN-subtracted host with a dust-attenuated SED fit. Including the upper limits, the observed Ly$\alpha$ follows the Ly$\alpha$ production in this host model more closely than it follows H$\alpha$/UV, in both equivalent width and luminosity. Every detection exceeds its host-model value by a factor of 1.5–18, leaving room for a nuclear contribution. The black hole is visible in these sources, but the Ly$\alpha$ we observe is more closely tied to its host. The median effective Ly$\alpha$ escape fraction of the detections is only 0.09, which suggests that ionizing escape from CBEs is typically modest and varies widely.

*Keywords:* Active galactic nuclei (16), High-redshift galaxies (734), Lyman-alpha galaxies (978), Reionization (1383)

## 1. INTRODUCTION

JWST has revealed a large population of faint broad-line active galactic nuclei (AGN) at $z > 4$ (e.g., J. Matthee et al. 2024; I. Juodžbalis et al. 2026; J. Zhang et al. 2026; X. Lin et al. 2025, 2026a). Most are identified through broad H$\alpha$ emission from dense gas moving at thousands of km s$^{-1}$ near an accreting black hole. Many are also X-ray weak and show little variability, which keeps their physical nature under debate (M. Yue et al. 2024; R. Maiolino et al. 2024; M. Kokubo & Y. Harikane 2025; J. E. Greene et al. 2025). A prominent subset, the little red dots (LRDs), pairs compact red rest-optical continua with blue rest-UV emission. LRDs have been studied through their identification, sizes, number densities, and dust emission (J. F. W. Baggen et al. 2024; P. G. Pérez-González et al. 2024; C. C. Williams et al. 2024; Y. Ma et al. 2025; I. Delvecchio et al. 2025; J. Ding et al. 2026), black-hole and host masses (I. Juodžbalis et al. 2025; B. L. Jones et al. 2025; L. R. Ivey et al. 2026), rest-UV and rest-optical spectra (H. B. Akins et al. 2024; P. Rinaldi et al. 2025a; K. Davis et al. 2026; B. Wang et al. 2026), low-redshift analogs (C. J. Burke

Email: yongdaz@arizona.edu
* These authors contributed equally to the analysis in this work.

et al. 2025; P. Rinaldi et al. 2025b; X. Lin et al. 2026b,c), and possible origins and descendants (J. Jeon et al. 2025; S. Obuchi et al. 2026; Y. Zhong et al. 2026). If these AGN are common and their ionizing photons escape efficiently, they could contribute substantially to the ionizing background during reionization. Whether their Ly$\alpha$ and Lyman-continuum (LyC) photons escape depends on gas beyond the visible broad-line region (BLR).

Ly$\alpha$ traces high-redshift galaxies and the ionization state of the intergalactic medium (IGM; e.g., C. A. Mason et al. 2018; Z. Chen et al. 2026a; M. Tang et al. 2024a; H. M. Christenson et al. 2023; S. Hashemi et al. 2025). Ly$\alpha$ and LyC photons may escape through the same low-column-density, low-attenuation channels, and observations and simulations find a broad connection between their escape fractions (X. Lin et al. 2024; R. Begley et al. 2024; N. Choustikov et al. 2024). The observed Ly$\alpha$ also depends on transfer through neutral gas, dust, the circumgalactic medium (CGM), and the IGM (e.g., P. Bolan et al. 2022; Z. Chen et al. 2026b), so it is a useful but indirect probe of LyC escape (for reviews, see M. Ouchi et al. 2020; M. J. Hayes & C. Scarlata 2023). In the Case B limit, the intrinsic Ly$\alpha$/H$\alpha$ ratio is fixed to first order (D. E. Osterbrock & G. J. Ferland 2006), although optically thick or density-bounded gas can move it away from Case B (C. Scarlata et al. 2024; W. McClymont et al. 2025). Because JWST measures both H$\alpha$ and Ly$\alpha$ in AGN at $z > 4$, broad-line AGN offer a direct test of whether strong nuclear recombination emission comes with strong observed Ly$\alpha$. A type-1 view shows the BLR along one sightline, but Ly$\alpha$ photons scatter through gas from nuclear to intergalactic scales and need not escape along the same path.

Recent JWST observations show that the two can differ. LRDs and other broad-line sources can have strong broad Balmer emission but weak, narrow, or spatially extended Ly$\alpha$ (A. Torralba et al. 2026; Z. Ji et al. 2026a), and broad Ly$\alpha$ is uncommon even when broad H$\alpha$ is clearly present (Y. Kageura et al. 2026). Some LRDs may still have a BLR contribution: a stacked medium-resolution spectrum shows a broad Ly$\alpha$ wing that matches broad H$\alpha$ (S. Geris et al. 2026). Compact blue broad-line sources, or little blue dots (LBDs; P. Madau & R. Maiolino 2026), show higher Ly$\alpha$ visibility, possibly through lower gas columns (S. Mascia et al. 2026). LRD selections still differ between studies, which use different color cuts or continuum-slope criteria (J. E. Greene et al. 2024; V. Kokorev et al. 2024; D. D. Kocevski et al. 2025; H. B. Akins et al. 2025; K. N. Hainline et al. 2025; J. Zhang et al. 2026), and spectroscopic LRD samples are heterogeneous (A. de Graaff et al. 2025a; P. G. Pérez-González et al. 2026). To avoid depending on a particular LRD definition, we refer to LRDs, LBDs, and other broad-line AGN collectively as compact broad-line emitters (CBEs). This umbrella term spans the full range of continuum colors and is broader than the blue CBE selection of S. Mascia et al. (2026); we select our sample on broad H$\alpha$ alone.

The largest study so far analyzed 110 LRDs with NIRSpec PRISM spectra (Z. Ji et al. 2026a). It finds that Ly$\alpha$/H$\alpha$ lies below that of star-forming galaxies and that Ly$\alpha$ luminosity tracks [O III] luminosity, which suggests that Ly$\alpha$ is tied to the host rather than to the compact broad-line source. Two questions remain open. At PRISM resolution, the Ly$\alpha$ line width cannot be compared with the broad-H$\alpha$ width, and [O III] can be excited by both star formation and the AGN (V. Sok et al. 2026; S. Geris et al. 2026), so it may not fully isolate the host.

In this paper, we ask which component of a CBE is most closely related to the Ly$\alpha$ that we observe. Broad H$\alpha$ traces the visible broad-line nucleus. AGN-subtracted imaging and spectral energy distribution (SED) fitting give an independent view of the host galaxy, which in LRDs is often faint, extended, or offset from the compact source (C.-H. Chen et al. 2025b,a; P. Rinaldi et al. 2025c). We use the Deep Insights into UV Spectroscopy at the Epoch of Reionization (DIVER) survey to measure Ly$\alpha$ in 12 CBEs at $z = 4.17$–$5.54$, mostly from medium-resolution G140M spectra that resolve line widths well below those of broad H$\alpha$. We test whether Ly$\alpha$ follows H$\alpha$, whether it shares the broad-H$\alpha$ line width, and whether it follows the Ly$\alpha$ in the AGN-subtracted host SED model. Section 2 describes the data and measurements, Section 3 presents the results, Section 4 discusses the origin of the observed Ly$\alpha$ and the implications for ionizing escape, and Section 5 summarizes our findings. We adopt the Planck 2018 flat $\Lambda$CDM cosmology as implemented in Astropy ($H_0 = 67.66$ km s$^{-1}$ Mpc$^{-1}$, $\Omega_{\rm m} = 0.310$; Planck Collaboration et al. 2020). All magnitudes are in the AB system.

## 2. DATA AND MEASUREMENTS

### 2.1. *DIVER spectroscopy*

DIVER (JWST PID 8018; PI: X. Lin) is a NIRSpec multi-object spectroscopic survey of GOODS-N, with median exposure times of 20.4 hr in F070LP/G140M and 2.3 hr in PRISM. Target selection and slit allocation did not use prior information on Ly$\alpha$. The reduction follows Y. Zhu et al. (2026a), with the DIVER-specific updates of Y. Zhu et al. (2026b). These updates extend the F070LP/G140M wavelength coverage to $\simeq 3$ $\mu$m, using the flat-field and sensitivity calibration of J. Scholtz et al. (2025). With this calibration, fluxes agree with those from the other gratings within 10%. The pipeline treats the nodded MSA spectra as point sources and applies the standard point-source path-loss correction for the planned intra-shutter position. We extract 1D spectra in a six-pixel ($\approx 0.6''$) aperture and apply no further aperture correction or scaling to imaging. Ly$\alpha$ is likely more extended than the UV continuum. Emission scattered outside the $0.2''$ shutter or removed by the nodded

**Table 1.** CBE sample and Lyα constraints

| ID | $z$ | Spectrum | $F_{\mathrm{Ly}\alpha}$ | $\mathrm{EW}_{\mathrm{Ly}\alpha}$ | $\log f^{\mathrm{eff}}_{\mathrm{esc,Ly}\alpha}$ | $\log L_{\mathrm{H}\alpha,\mathrm{total}}$ | $\mathrm{FWHM}_{\mathrm{H}\alpha,\mathrm{broad}}$ | $\mathrm{FWHM}_{\mathrm{Ly}\alpha,\mathrm{obs}}$ |
|---|---|---|---|---|---|---|---|---|
| 1029154 | 4.17 | PRISM | $< 2.88$ | $< 59$ | $< -1.80$ | 42.57 | 2003 | ··· |
| 1086784 | 4.405 | G140M-2 | $< 1.47$ | $< 30$ | $< -1.84$ | 42.37 | 3179 | ··· |
| 1008411 | 4.41 | G140M-2 | $8.43 \pm 1.61$ | $273 \pm 71$ | $-0.99$ | 42.28 | 3281 | 424 |
| 1008671 | 4.41 | G140M-2 | $< 10.17$ | $< 127$ | $< -1.28$ | 42.65 | 2272 | ··· |
| 1086855 | 4.41 | G140M-2 | $11.52 \pm 0.64$ | $360 \pm 72$ | $-1.11$ | 42.53 | 1724 | 961 |
| 1033320 | 4.48 | PRISM | $< 8.86$ | $< 116$ | $< -0.91$ | 42.24 | 1951 | ··· |
| 1020621 | 4.681 | G140M-2 | $10.25 \pm 0.40$ | $216 \pm 57$ | $-0.88$ | 42.32 | 1605 | 316 |
| 1034620 | 5.19 | G140M-1 | $11.56 \pm 0.42$ | $73 \pm 4$ | $-1.20$ | 42.80 | 1077 | 512 |
| 1077652 | 5.229 | G140M-1 | $< 1.10$ | $< 20$ | $< -1.68$ | 42.26 | 1026 | ··· |
| 9994014 | 5.23 | G140M-1 | $< 0.70$ | $< 10$ | $< -2.38$ | 42.77 | 2084 | ··· |
| 1020514 | 5.36 | G140M-1 | $161.9 \pm 2.6$ | $693 \pm 19$ | 0.08 | 42.70 | 1612 | 585 |
| 1087388 | 5.54 | G140M-1 | $1.79 \pm 0.25$ | $24 \pm 4$ | $-2.80$ | 43.65 | 2964 | 665 |

Note—Lyα fluxes are in $10^{-18}$ erg s$^{-1}$ cm$^{-2}$, EWs are rest-frame Å, FWHMs are in km s$^{-1}$, and luminosities are in erg s$^{-1}$. Limits are $2\sigma$. G140M-1 and G140M-2 denote first- and second-order G140M; PRISM is first order. $\mathrm{FWHM}_{\mathrm{Ly}\alpha,\mathrm{obs}}$ includes instrumental broadening (Section 3.3). $f^{\mathrm{eff}}_{\mathrm{esc,Ly}\alpha}$ uses total Hα. Broad-Hα FWHMs are from J. Zhang et al. (2026) and I. Juodžbalis et al. (2026).

background subtraction is therefore potentially missed, and line fluxes and EWs might be biased low. L. Napolitano et al. (2026) found an average NIRSpec Lyα slit loss of $35 \pm 10\%$ at $z \simeq 6$. All sources are reduced and measured in the same way, so this bias affects relative comparisons less than absolute values.

F070LP/G140M covers first-order Lyα at $z \gtrsim 4.8$. At lower redshift, Lyα is recorded in second order at an apparent wavelength $\lambda_{\mathrm{app}} = 2 \times 1215.67\,(1+z)$ Å. This falls in the extended range, whose calibration assumes first-order light. We convert second-order line fluxes to true fluxes with the ratio of the first- and second-order sensitivity curves of msaexp (G. Brammer 2023) and the wavelength Jacobian, $d\lambda_{\mathrm{app}} = 2\,d\lambda_{\mathrm{true}}$, for apparent wavelengths of 1.30–2.00 $\mu$m. The conversion factors for our five second-order measurements are 3.19–5.05, and a $\pm 0.002$ $\mu$m shift in apparent wavelength changes them by $\lesssim 4\%$. We test the conversion with sources at $z > 4.8$, whose Lyα appears in both orders of the same G140M spectrum. For the 13 with second-order S/N $\geq 5$, at true wavelengths of 0.75–0.98 $\mu$m, the converted second-order fluxes are a median of 1.01 times the first-order fluxes (16th–84th percentiles 0.69–1.94). Our second-order lines lie at 0.66–0.69 $\mu$m, where the second-order sensitivity rises steeply, so individual fluxes may be uncertain by a factor of $\sim 2$. Halving or doubling them does not change our conclusions (Sections 3.2 and 4.2). PRISM gives only marginal Lyα fluxes for 1086855 and 1008411 (S/N of 2.8 and 1.1), 0.5 and 0.2 times the converted values. Near the blue end of PRISM, Lyα fluxes of other DIVER sources scatter widely and include significantly negative values, so we do not use PRISM to test the conversion.

### 2.2. *Sample*

The sample contains the 12 sources with secure broad Hα in the CONGRESS/FRESCO census of J. Zhang et al. (2026) and the JADES census of I. Juodžbalis et al. (2026) that have usable DIVER Lyα coverage (Table 1). We restrict the sample to $z < 6$, because IGM attenuation of Lyα rises steeply at higher redshift (e.g., G. C. Jones et al. 2025; Y. Zhu et al. 2026b; Z. Chen et al. 2026a). Our test requires a directly visible BLR, so the sample excludes photometric LRD candidates without broad-line spectroscopy and narrow-line AGN. J. Zhang et al. (2026) identify the LRDs among these broad-Hα emitters with color selections (see also D. D. Kocevski et al. 2025) and find that 42%–47% of them are not LRDs. We analyze the CBEs as one population and do not classify individual objects.

### 2.3. *Lyα measurements*

Figure 1 shows the Lyα spectra of the 12 CBEs. We measure first-order G140M Lyα following Y. Zhu et al. (2026b). A local continuum is fitted outside the line, and the line peak is located within $\pm 1000$ km s$^{-1}$ of the systemic redshift. The continuum-subtracted flux is summed within $\pm 16$ Å (observed frame; $\approx \pm 600$ km s$^{-1}$) of the peak. A line is detected if both the integrated and peak signal-to-noise ratios are $\geq 3$. Second-order fluxes are summed within $\pm 2500$ km s$^{-1}$ after subtracting the median continuum at $+4000$ to $+9000$ km s$^{-1}$, and then converted. For PRISM, we subtract a clipped red-side continuum at rest-frame 1350–1500 Å and integrate over 1170–1270 Å. Nondetections are reported as $2\sigma$ upper limits. We adopt PRISM for 1029154, whose second-order Lyα falls at 1.257 $\mu$m, below the calibrated range, and for 1033320, whose second-order Lyα falls in a spectral gap.

The rest-frame $\mathrm{EW}_{\mathrm{Ly}\alpha}$ divides the line flux by the continuum at rest-frame 1300 Å from the best-fit SED of the total (AGN+host) photometry (Y. Zhu et al. 2026b); the continuum is largely undetected in the grating spec-

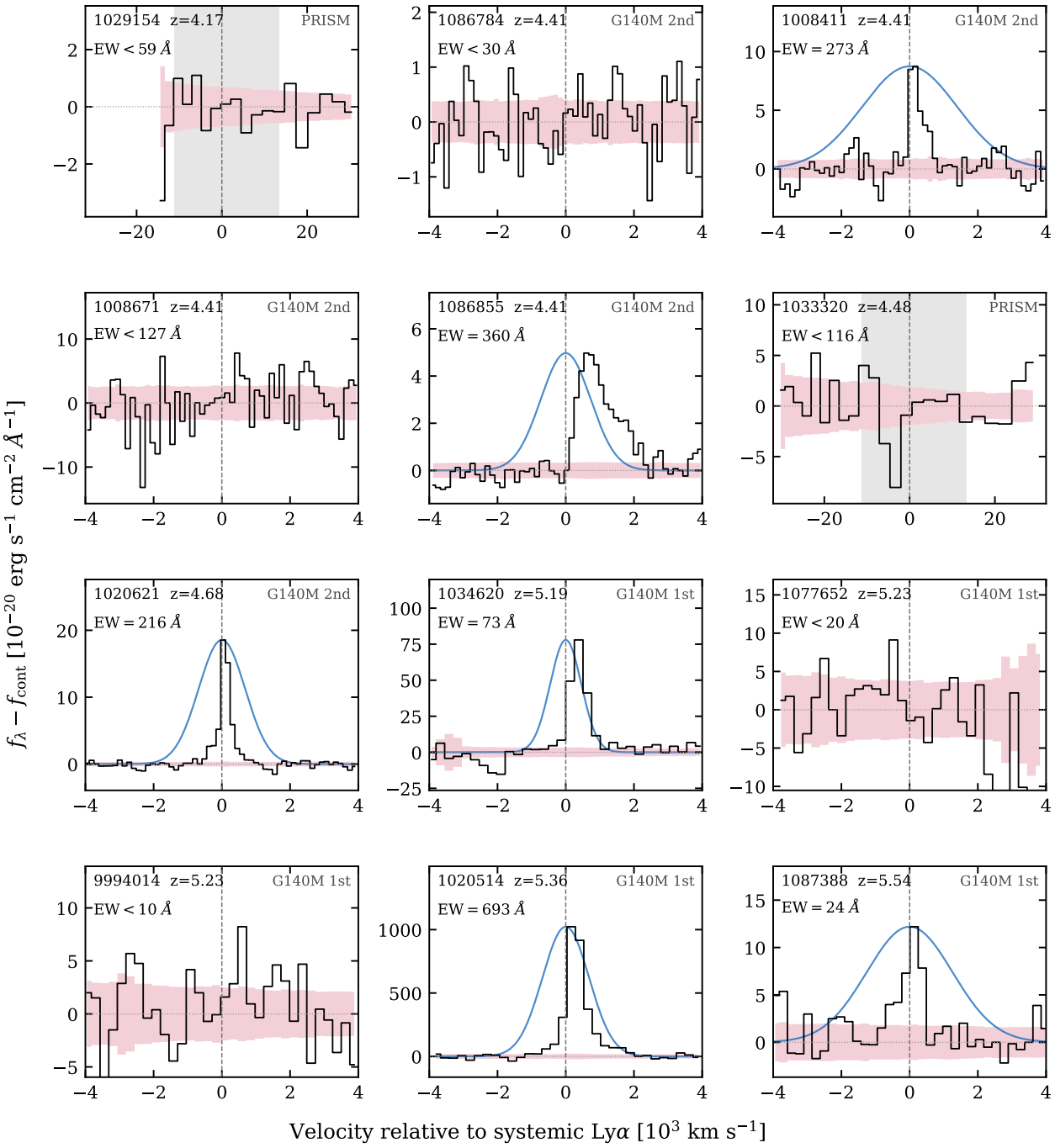



**Figure 1.** Ly$\alpha$ spectra of the 12 CBEs, ordered by redshift, in velocity relative to the systemic (H$\alpha$) redshift. Labels give the adopted spectrum and the rest-frame $\mathrm{EW}_{\mathrm{Ly}\alpha}$ ($2\sigma$ limits for nondetections). Pink bands show the $1\sigma$ uncertainty, and the local continuum is subtracted. G140M panels span $\pm$4000 km s$^{-1}$; second-order panels show the apparent, first-order-calibrated flux density, while the adopted line fluxes include the order-dependent response conversion. For G140M detections, blue curves show a Gaussian with the broad-H$\alpha$ FWHM at the systemic velocity, scaled to the Ly$\alpha$ peak. The two PRISM panels span $\pm$32,000 km s$^{-1}$, and the gray band marks the rest-frame 1170–1270 Å integration window. For 1033320, second-order G140M Ly$\alpha$ falls in a spectral gap, and we adopt the PRISM constraint.

tra. For 1034620, which lacks an SED fit, we use the PRISM red-side continuum.

We define the effective Ly$\alpha$ escape fraction

$$f_{\mathrm{esc,Ly}\alpha}^{\mathrm{eff}} = \frac{L_{\mathrm{Ly}\alpha}}{8.7\, L_{\mathrm{H}\alpha}}, \tag{1}$$

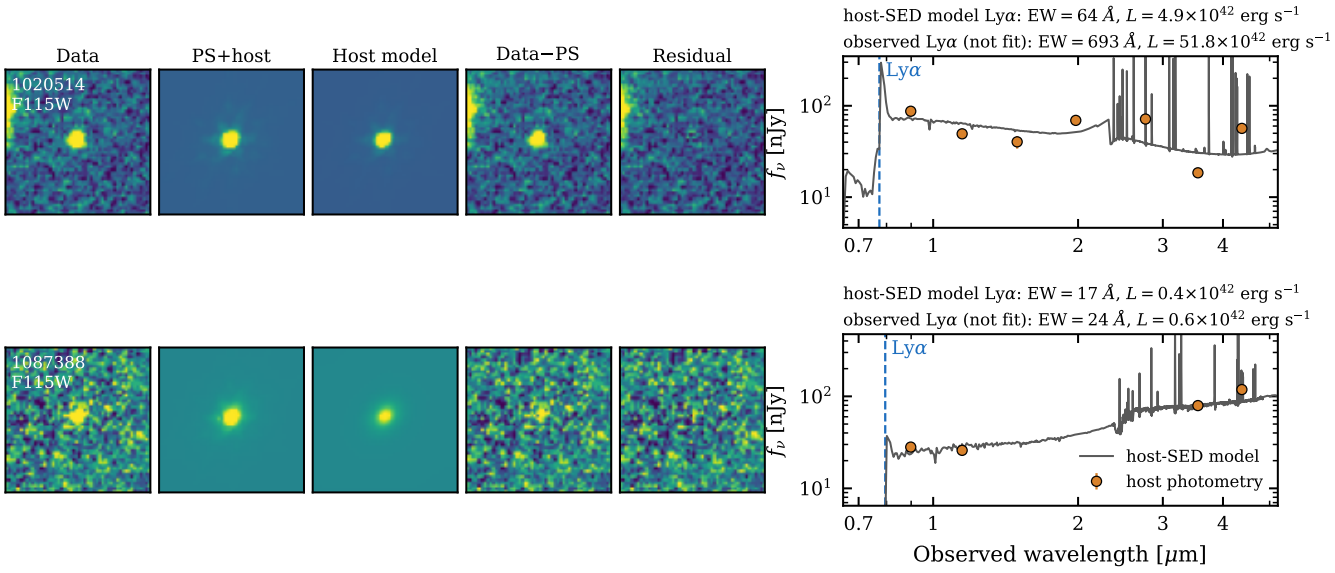



**Figure 2.** AGN–host decomposition and host SED for a strong (1020514, top) and a weak (1087388, bottom) Lyα detection. Left: F115W data, the PS+host model, the Sérsic host model, the data after PS subtraction, and the residual (Z. Ma et al. 2026); each panel has its own display stretch. Right: AGN-subtracted host photometry (orange) and the best-fit host SED model (gray), with the Lyα wavelength marked; 1087388 has no JADES F150W, F200W, or F277W imaging, so its host photometry has four bands. The annotations compare the Lyα in the host SED model with the observed Lyα, which is not used in the fit.

where $L_{\mathrm{H}\alpha}$ is the total (broad+narrow) Hα luminosity, not corrected for dust, and 8.7 is the Case B Lyα/Hα ratio (D. E. Osterbrock & G. J. Ferland 2006) for $T_e = 10^4$ K and $n_e \approx 350$ cm$^{-3}$ (M. Hayes 2015). $f^{\mathrm{eff}}_{\mathrm{esc,Ly}\alpha}$ is an empirical visibility ratio that includes radiative transfer in the nucleus and host, CGM and IGM transmission, aperture effects, and the Hα normalization. Total Hα is from the NIRCam grism measurements of J. Zhang et al. (2026). For the JADES sources 1020621 and 1077652, we fit narrow and broad Hα and [N II] in the public JADES G395M spectra (F. D'Eugenio et al. 2025); the narrow component carries about two-thirds of the Hα flux of 1020621. For 1020514, $f^{\mathrm{eff}}_{\mathrm{esc,Ly}\alpha} = 1.20$; the aperture mismatch between the slit Lyα and slitless Hα measurements and departures from Case B, such as collisional enhancement of Lyα, may contribute.

### 2.4. *Host decomposition and host-model Lyα*

We fit the AGN–host decomposition of all 12 sources in the JADES Data Release 5 (DR5) NIRCam images and catalogs (D. J. Eisenstein et al. 2023; B. D. Johnson et al. 2026; B. E. Robertson et al. 2026), generally following Z. Ma et al. (2026) (Figure 2). The AGN is modeled with the JADES mosaic point-spread function (PSF) and the host with a single PSF-convolved Sérsic profile. To improve the host characterization, we fit the short-wavelength bands jointly, with one Sérsic shape and one AGN–host offset shared across them. A Markov chain Monte Carlo fit then gives the point-source (PS) and host fluxes in each band. We fit the host photometry with Prospector (B. D. Johnson et al. 2021) and FSPS (C. Conroy et al. 2009), using the model of Y. Zhu et al. (2026b, Section 2.4). The model assumes a G. Chabrier (2003) initial mass function and a seven-bin nonparametric star-formation history with the continuity prior of J. Leja et al. (2019). It includes the flexible dust law of M. Kriek & C. Conroy (2013) with extra attenuation of young stars (S. Charlot & S. M. Fall 2000), nebular emission (N. Byler et al. 2017), dust emission (B. T. Draine & A. Li 2007), and a mid-infrared AGN component. The redshift may vary within ±0.01 of the spectroscopic value, and the model photometry is computed with the neural-network emulator of E. P. Mathews et al. (2023). The fitted photometry begins at F090W, redward of Lyα for all sources except 1087388, whose Lyα red wing falls at the blue edge of F090W and contributes $\lesssim 4\%$ of that band. Neither the spectroscopic Lyα nor Hα enters the fit.

The host-model Lyα is the Lyα emission in the dust-attenuated best-fit host SED model. We integrate the positive excess above a power-law continuum, fitted at rest-frame 1275–1305 and 1325–1365 Å, over 1215–1270 Å, and convert it to an EW and a luminosity. The model includes dust attenuation but no Lyα resonant transfer through neutral gas, the CGM, or the IGM, so the host-model Lyα traces Lyα production in the host. The model is sampled at ≈ 10 Å near Lyα, so the integration is approximate. The host model of 1086784 has no coherent Lyα excess, and we omit it from the host comparison.

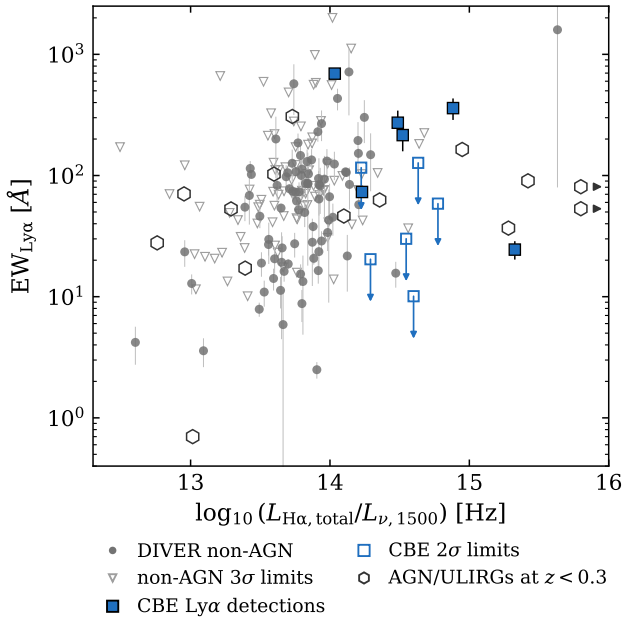



**Figure 3.** Ly$\alpha$ EW versus H$\alpha$/UV. Both samples use total H$\alpha$ and the observed total $L_{\nu,1500}$. Gray circles and open triangles show DIVER non-AGN detections and 3$\sigma$ upper limits. Blue filled squares show CBE Ly$\alpha$ detections, and open squares with arrows show 2$\sigma$ upper limits. Error bars show 1$\sigma$ EW uncertainties. Open hexagons show Ly$\alpha$-detected AGN and ULIRGs at $z < 0.3$ from W. Liu et al. (2022), whose UV continuum is measured near 1125 Å, so their positions are approximate. Two of them, at $\log(L_{\rm H\alpha}/L_\nu) = 16.2$ and 16.7, are shown at the right edge with arrows.

### 2.5. *Non-AGN comparison sample*

The comparison sample is the 250 non-AGN galaxies in the DIVER Ly$\alpha$ sample of Y. Zhu et al. (2026b), measured with the same spectra and methods. None of the CBEs are in this sample. We use the 173 galaxies with H$\alpha$ and UV measurements: 84 Ly$\alpha$ detections and 89 3$\sigma$ upper limits, as in Y. Zhu et al. (2026b). At the 2$\sigma$ level used for the CBEs, these limits would be a factor of 1.5 lower.

## 3. RESULTS

The 12 sources include six Ly$\alpha$ detections and six 2$\sigma$ upper limits, a detection fraction of 0.50 (68% binomial confidence interval 0.36–0.64). Non-AGN galaxies at the same redshifts have a similar detection fraction of 0.40 (34 of the 86 with Ly$\alpha$ measurements at $z = 4.17$–$5.54$; 0.34–0.45). The detections span EW$_{\rm Ly\alpha}$ = 24–693 Å, and the limits span EW$_{\rm Ly\alpha} < 10$ to $< 127$ Å.

### 3.1. *Strong H$\alpha$ does not predict strong Ly$\alpha$*

Figure 3 shows EW$_{\rm Ly\alpha}$ as a function of $L_{\rm H\alpha}/L_{\nu,1500}$, where both samples use total H$\alpha$ and the observed total UV continuum. The CBEs have higher H$\alpha$/UV than most DIVER non-AGN galaxies, but larger H$\alpha$/UV does not imply stronger Ly$\alpha$. Source 1087388 has the largest H$\alpha$ luminosity and H$\alpha$/UV in the sample but EW$_{\rm Ly\alpha}$ = 24 Å, while 1020514 has the strongest Ly$\alpha$ at the lowest H$\alpha$/UV among the CBEs.

Both axes are normalized by the UV continuum, so some positive covariance is expected. A fit to the 84 non-AGN detections gives

$$\log \mathrm{EW}_{\rm Ly\alpha} = a + b \log(L_{\rm H\alpha}/L_{\nu,1500}), \qquad (2)$$

with $a = -8.719$ and $b = 0.757$. The six CBE detections scatter around this relation, with a median residual of +0.03 dex and individual residuals from −1.49 to +0.94 dex. Five of the six upper limits lie 0.25–1.33 dex below the relation, and the PRISM limit for 1033320 lies on it. At high H$\alpha$/UV, the CBEs span a wide range of Ly$\alpha$ strength, and several lie well below the non-AGN relation. The 14 Ly$\alpha$-detected AGN and ULIRGs at $z < 0.3$ from W. Liu et al. (2022) show the same behavior: nine lie below the relation (median residual −0.32 dex), and all five with $\log(L_{\rm H\alpha}/L_\nu) > 14.9$ lie 0.4–2.0 dex below it. We find no clear trend between EW$_{\rm Ly\alpha}$ and UV luminosity, total H$\alpha$ luminosity, or broad-H$\alpha$ FWHM among the six detections (Spearman rank coefficient $|\rho| \leq 0.49$, $p$-value $\geq 0.36$).

### 3.2. *Observed Ly$\alpha$ and host-model Ly$\alpha$*

Because the Ly$\alpha$ strength does not follow H$\alpha$/UV, we turn to the host galaxy. Figure 4 compares the observed and host-model Ly$\alpha$ for the 11 sources with a host-model value (six detections and five upper limits). The observed Ly$\alpha$ tends to rise with the host-model Ly$\alpha$, more clearly in EW than in luminosity, but not with H$\alpha$/UV.

To include the upper limits, we use the generalized Kendall rank correlation coefficient $\tau$ (T. Isobe et al. 1986), which runs from −1 to +1 like Spearman $\rho$ and uses only pairs of sources whose order is unambiguous; $p$-values come from random permutations. The host model gives $\tau = 0.37$ ($p = 0.14$) in EW and $\tau = 0.26$ ($p = 0.31$) in luminosity, whereas H$\alpha$/UV gives $\tau = -0.19$ ($p = 0.44$). In bootstrap resamplings, the host relation has the larger $\tau$ in 88% of cases in EW (against H$\alpha$/UV) and in 77% in luminosity (against broad-H$\alpha$ luminosity, $\tau = 0.04$). These fractions are 71%–93% when we drop 1034620 and 9994014, whose decompositions are affected by a foreground neighbor and image artifacts (Z. Ma et al. 2026), or halve or double the second-order fluxes. A linear fit that treats the upper limits as censored values gives a positive slope of observed on host-model EW (one-sided permutation $p = 0.03$), whereas H$\alpha$/UV gives none ($p = 0.67$). With the slope fixed at unity, the host model predicts the observed EW with a scatter of 0.66 dex, compared with 1.05 dex for H$\alpha$/UV; in luminosity, the scatter is 0.81 dex for the host model and 1.07 dex for Case B H$\alpha$. With 11 sources, this preference is not yet decisive. The

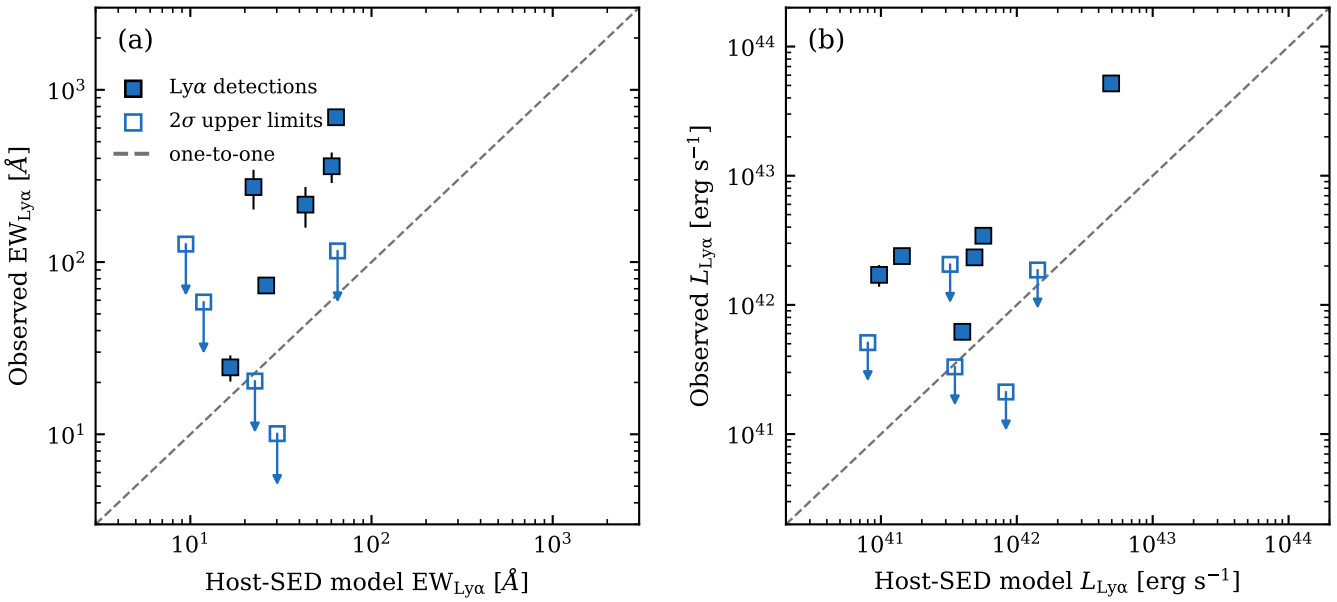



**Figure 4.** Observed Lyα versus the Lyα emission in the dust-attenuated best-fit host SED model, in (a) EW and (b) luminosity. The host model uses neither the spectroscopic Lyα nor photometry containing Lyα. Filled squares show the six detections with $1\sigma$ error bars, and open squares with arrows show $2\sigma$ upper limits. The dashed line marks equality. 1086784 has no coherent host-model Lyα and is omitted.

six detections alone give the same picture: Spearman $\rho = 0.83$ ($p = 0.058$) for the host model and $\rho = -0.49$ ($p = 0.36$) for Hα/UV.

Every detection lies above the one-to-one relation, by factors of 1.5–18. Because the host model already includes dust attenuation and resonant transfer usually reduces Lyα further, the excess implies additional Lyα from outside the stellar host component, possibly from the AGN, or host Lyα production that the SED fit underestimates. The host models also underpredict narrow Hα. Their dust-attenuated Hα is a median of 0.3 (range 0.06–1.15) of the observed narrow Hα. Part of the narrow-line emission may therefore arise outside the stellar host component, or the fit may miss some star formation. Conversely, 9994014 lies at least a factor of 4 below its host-model luminosity, so host Lyα production alone does not guarantee visible Lyα.

Figure 2 shows the two ends of the sample, 1020514 and 1087388. In both, the host accounts for most of the rest-frame 1500 Å light (75% and 64%), and the point source dominates the rest-frame optical. Their host-model EWs are 64 and 17 Å, and their observed EWs are 693 and 24 Å. The host of 1020514 is young, low-mass, and nearly dust-free (mass-weighted age ≈ 30 Myr, $\log M_*/M_\odot = 7.9$, and diffuse dust optical depth $\tau_V = 0.01$), whereas the host of 1087388 is older, more massive, and dustier (≈ 400 Myr, 9.2, and 0.36). Host age alone does not set the Lyα strength, however: among the detections, the oldest host, 1008411 (≈ 550 Myr), has EW$_{Lyα}$ = 273 Å.

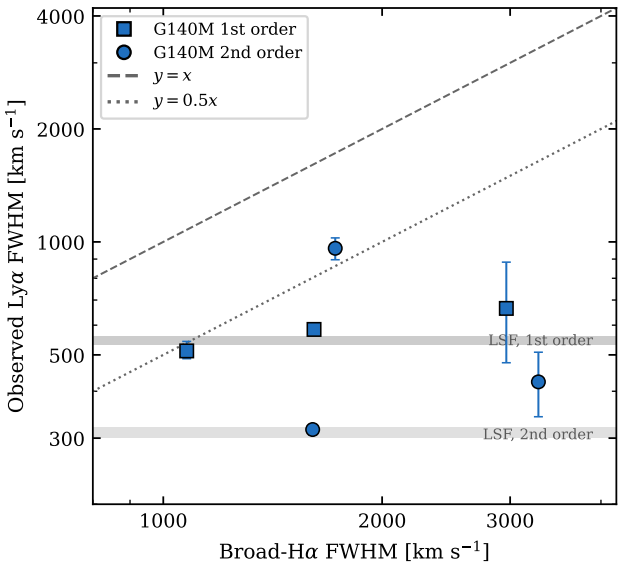



**Figure 5.** Observed Lyα FWHM versus broad-Hα FWHM for the six detections, from first-order (squares) and second-order (circles) G140M spectra. The Lyα widths include instrumental broadening; gray bands mark the nominal instrumental FWHM for each order. The dashed line marks equal widths, and the dotted line marks $y = 0.5x$, the approximate apparent width of a BLR-width line whose blue half is absorbed.

### 3.3. *Lyα is narrower than broad Hα*

If the observed Lyα came directly from the BLR, we would expect it to be about as broad as broad Hα. Figure 5 shows that it is not: every detected Lyα line is narrower than broad Hα, with observed FWHMs of 316–961 km s$^{-1}$ against 1077–3281 km s$^{-1}$, a ratio of 0.13–0.56. These Gaussian-fit widths include instrumental broadening (about 530–560 km s$^{-1}$ in first order and 300–320 km s$^{-1}$ in second order), so the intrinsic lines are narrower still; three lines (1020621, 1034620, and 1020514) are at most marginally resolved.

Two effects could make BLR Lyα look narrower. First, neutral gas can absorb the blue half of the line, roughly halving its apparent width (dotted line in Figure 5). Only 1086855 lies above this line. Its Lyα is the broadest in the sample (FWHM = 961±64 km s$^{-1}$, peak redshifted by ≈ 800 km s$^{-1}$) but still narrower than its broad Hα (1724 km s$^{-1}$). This line may reflect clumpy neutral gas or a favorable escape path, as inferred for an LRD with broad Lyα in SPURS (M. Tang et al. 2026). Second, a faint broad component could hide beneath a bright narrow core. When we add a systemic component with the broad-Hα width, five lines do not need it ($2\sigma$ limits of 10–49% of the narrow-line flux). Only 1020514, the brightest line, prefers a broad red wing with ≈ 40% of the narrow-line flux, which may be a weak nuclear contribution or a red scattering wing. S. Geris et al. (2026) detect a broad Lyα component in a stacked medium-resolution spectrum of eight LRDs; because a stack averages over sources, such a component could arise in a subset of objects like 1020514.

Lyα produced or scattered away from the nucleus could also be offset along the slit. In the 2D spectra, the Lyα and continuum positions agree within 0.14″ (≤ 1 kpc) for all six detections; the formal 0.024″ offset of 1020621, in second-order data, drops to $2.4\sigma$ when we allow for a 0.1-pixel systematic uncertainty.

## 4. DISCUSSION

### 4.1. *What sets the observed Lyα*

Every source in our sample has a directly visible BLR, yet the Lyα strength does not follow the Hα luminosity or Hα/UV. Other broad-line samples also show weak or mostly narrow Lyα (A. Torralba et al. 2026; Y. Kageura et al. 2026). In 110 LRDs at $z \geq 4$, Z. Ji et al. (2026a) find Lyα luminosities and EWs similar to those of star-forming galaxies but systematically lower Lyα/Hα. Our CBEs show this deficit mainly through their nondetections: the detections scatter around the non-AGN relation in Figure 3, while five of the six upper limits lie below it. AGN and ULIRGs at $z < 0.3$ also lie at or below this relation, which suggests that AGN do not generally have higher Lyα visibility than star-forming galaxies. Within that sample, Lyα EW increases with AGN luminosity and AGN fraction (W. Liu et al. 2022); we find no such trend with Hα luminosity.

Two processes can separate the observed Lyα from the BLR. First, dense nuclear gas can change the intrinsic Lyα/Hα ratio: Balmer-continuum opacity, enhanced $n = 2$ populations, collisional effects, and electron scattering can drive it far from Case B (J. C. Shields & G. J. Ferland 1993). In LRDs, such dense gas may also produce the observed Balmer breaks and Balmer absorption (K. Inayoshi & R. Maiolino 2025; R. P. Naidu et al. 2025; A. de Graaff et al. 2025b,a), and the broad Balmer profiles may partly reflect radiative transfer through it rather than BLR kinematics alone (J. Matthee et al. 2026). Second, Lyα is resonantly transferred through the nucleus, host, and CGM. The neutral-gas covering fraction, dust, and velocity structure shape the emerging line (e.g., M. Gronke et al. 2017), and gas velocities move Lyα into regions of higher or lower IGM transmission (C. Cain et al. 2025). A high covering fraction can suppress Lyα even when the BLR is seen through a lower-opacity sightline. In LRDs, enhanced broad Hα relative to bolometric luminosity suggests high BLR covering factors and large gas columns (H. Yanagisawa et al. 2026), which would favor this suppression. Where Lyα does escape, it can do so through narrow channels. In LRD-204851, radiative-transfer modeling of the Lyα profile favors a low-column-density biconical cavity in a dense, slowly expanding neutral envelope (Z. Ji et al. 2026b), and narrow-line ratios in LRDs also point to lower-density channels through the gas envelope (V. Sok et al. 2026). The narrow line profiles (Section 3.3) suggest that the observed Lyα is largely shaped outside the BLR.

Observed Lyα follows the host-model Lyα more closely than Hα/UV (Section 3.2). Because the host model traces Lyα production in the host, this relation suggests that host star formation contributes to the observed line, although the host dust and gas that shape the host-model Lyα could also regulate the escape of nuclear Lyα. Z. Ji et al. (2026a) reach a similar conclusion by a different route. In their LRDs, Lyα luminosity tracks [O III] luminosity more closely than [O III] EW, and at $z \gtrsim 5.5$ the Lyα maps are often extended, asymmetric, and offset from the rest-optical light. They interpret these results as Lyα associated with the host-scale component rather than with the compact source of the broad lines and red continuum. In our 2D spectra, Lyα and continuum positions agree within 0.14″ along the slit (Section 3.3), but the 0.2″ shutter would miss emission extended or offset beyond it.

The excess above the host model leaves room for a nuclear contribution, which would also emerge narrow after transfer through host and CGM gas. We conclude that, in our sample, the observed Lyα of CBEs is more closely related to the host galaxy than to the BLR. Larger samples with deep rest-UV spectroscopy and Lyα maps will test this result beyond our six detections and five upper limits.

### 4.2. *Implications for ionizing escape*

Lyα visibility gives a rough guide to ionizing escape, because LyC leakers at $z \simeq 2$ show larger Lyα escape fractions, less dust, and lower neutral-gas columns (R. P. Naidu et al. 2022). At $z \simeq 5$–6, CGM and IGM transmission add scatter to this relation (M. Tang et al. 2024b). The six detections have a median $f^{\rm eff}_{\rm esc,Ly\alpha} = 0.091$, a 16th–84th percentile range of 0.051–0.35, and a full range of 0.0016–1.20; the upper percentile is set mainly by 1020514. Five of the six upper limits lie below the median, and the PRISM limit for 1033320 ($< 0.12$) lies above it. The detection-only median is an upper estimate of the characteristic escape scale; halving or doubling the second-order fluxes (Section 2.1) gives 0.057–0.18. Normalizing by narrow Hα alone, which carries 23–65% of the total, raises the individual values by factors of 1.6–4.2 and the detection median to 0.28.

D. Jiang et al. (2025) derive an upper bound on the AGN contribution to the ionizing budget at $z \approx 7.5$ that scales with the assumed LyC escape fraction:

$$\frac{\dot{N}^{\rm AGN}_{\rm ion}}{\dot{N}_{\rm ion,req}} \simeq 0.32 \left( \frac{f^{\rm LyC}_{\rm esc}}{0.75} \right). \tag{3}$$

Taking $f^{\rm eff}_{\rm esc,Ly\alpha} = 0.091$ as an approximate escape scale gives a contribution of about 3.9%, and the 16th–84th percentile range gives 2.2–15%; the narrow-Hα median gives about 12%. This scaling is approximate: the normalization refers to $z \approx 7.5$, our sample lies at $z \approx 4$–5.5, and $f^{\rm eff}_{\rm esc,Ly\alpha}$ measures Lyα visibility. If ionizing photons also escape through narrow low-column channels like that in LRD-204851 (Z. Ji et al. 2026b), the escape fraction depends on viewing angle, and our single sightline need not give the angle-averaged value. The star-forming-galaxy relation $f^{\rm LyC}_{\rm esc} \simeq 0.15 f^{\rm Ly\alpha}_{\rm esc}$ of R. Begley et al. (2024) would give an even smaller contribution of about 0.58%. Estimates in which AGN supply a much larger share, such as 31–75% at $z \simeq 5$–6 (M. Singha et al. 2025), depend on the adopted LyC escape fractions, which our data suggest are typically modest for CBEs. LRD ionizing spectra may also be softer than standard AGN spectra (B. Wang et al. 2025), and the timing of helium reionization limits how many LBDs can be highly super-Eddington (C. Cain et al. 2026). Our results support the conclusion of D. Jiang et al. (2025) and S. Mascia et al. (2026) that faint AGN are unlikely to dominate the ionizing photon budget during reionization.

## 5. SUMMARY

We measured Lyα in 12 CBEs at $z = 4.17$–5.54 with DIVER JWST/NIRSpec spectroscopy, finding six detections and six upper limits. We learn three things.

1. A visible BLR does not make Lyα bright: the Lyα strength does not follow Hα or Hα/UV.
2. The observed Lyα is unlikely to come directly from the BLR: every detected line is narrower than broad Hα.
3. Lyα is more closely tied to the host galaxy than to the nucleus, with room for a nuclear contribution.

The low Lyα visibility of these sources (median $f^{\rm eff}_{\rm esc,Ly\alpha} \approx 0.09$) suggests modest ionizing escape, so faint AGN are unlikely to dominate reionization. Deep rest-UV spectroscopy and Lyα maps of larger samples will show how host and nuclear Lyα combine.

## ACKNOWLEDGEMENTS

Y.Z. acknowledges support from the NIRCam Science Team contract to the University of Arizona, NAS5-02105. Y.Z. is also supported by JWST program #6434. L.K. acknowledges the support of a Royal Society University Research Fellowship (grant number URF\R1\251793). A.J.B. acknowledges funding from the "FirstGalaxies" Advanced Grant from the European Research Council under the European Union's Horizon 2020 research and innovation programme (grant agreement No. 789056). Support for program #6434 was provided by NASA through a grant from the Space Telescope Science Institute, which is operated by the Association of Universities for Research in Astronomy, Inc., under NASA contract NAS 5-03127. This manuscript benefited from language editing with ChatGPT (OpenAI, GPT-5.6 Sol), and the analysis code was developed with assistance from Claude Code (Anthropic, Claude Opus 5.5). All revised content and code were reviewed and verified by the authors.

This work is based on observations made with the NASA/ESA/CSA James Webb Space Telescope. The data were obtained from the Mikulski Archive for Space Telescopes at the Space Telescope Science Institute, which is operated by the Association of Universities for Research in Astronomy, Inc., under NASA contract NAS 5-03127 for JWST. These observations are associated with programs #8018 (DIVER), #1895 (FRESCO), #3577 (CONGRESS), and #1181 (JADES). JADES DR5 includes NIRCam data from JWST programs 1176, 1180, 1181, 1210, 1264, 1283, 1286, 1287, 1895, 1963, 2079, 2198, 2514, 2516, 2674, 3215, 3577, 3990, 4540, 4762, 5398, 5997, 6434, 6511, and 6541. JADES DR5 includes MIRI data from JWST programs 1180, 1181, and 1207. The authors acknowledge the teams of programs 1895, 1963, 2079, 2514, 3215, 3577, 3990, 6434, and 6541 for developing their observing program with a zero-exclusive-access period.

We respectfully acknowledge the University of Arizona is on the land and territories of Indigenous peoples. Today, Arizona is home to 22 federally recognized tribes, with Tucson being home to the O'odham and the Yaqui. The university strives to build sustainable relationships

with sovereign Native Nations and Indigenous communities through education offerings, partnerships, and community service.

## AUTHOR CONTRIBUTIONS

Y.Z. initiated and led this project, reduced the DIVER data, and led the interpretation. Z.M. performed the imaging decomposition and the host SED fitting. X.L. led the DIVER program. All authors contributed to the analysis and discussion.

*Facilities:* JWST (NIRSpec, NIRCam); MAST

*Software:* Astropy ( Astropy Collaboration et al. 2013, 2018, 2022), JWST Calibration Pipeline (H. Bushouse et al. 2025)

## REFERENCES


Akins, H. B., Casey, C. M., Berg, D. A., et al. 2024, doi: 10.48550/arXiv.2410.00949

Akins, H. B., Casey, C. M., Lambrides, E., et al. 2025, The Astrophysical Journal, 991, 37, doi: 10.3847/1538-4357/ade984

Astropy Collaboration, Robitaille, T. P., Tollerud, E. J., et al. 2013, Astronomy and Astrophysics, 558, A33, doi: 10.1051/0004-6361/201322068

Astropy Collaboration, Price-Whelan, A. M., Sip\H{o}cz, B. M., et al. 2018, The Astronomical Journal, 156, 123, doi: 10.3847/1538-3881/aabc4f

Astropy Collaboration, Price-Whelan, A. M., Lim, P. L., et al. 2022, The Astrophysical Journal, 935, 167, doi: 10.3847/1538-4357/ac7c74

Baggen, J. F. W., van Dokkum, P., Brammer, G., et al. 2024, The Astrophysical Journal, 977, L13, doi: 10.3847/2041-8213/ad90b8

Begley, R., Cullen, F., McLure, R. J., et al. 2024, Monthly Notices of the Royal Astronomical Society, 527, 4040, doi: 10.1093/mnras/stad3417

Bolan, P., Lemaux, B. C., Mason, C., et al. 2022, Monthly Notices of the Royal Astronomical Society, 517, 3263, doi: 10.1093/mnras/stac1963

Brammer, G. 2023, Zenodo, doi: 10.5281/zenodo.7299500

Burke, C. J., Stone, Z., Shen, Y., & Jiang, Y.-F. 2025, arXiv, doi: 10.48550/arXiv.2511.16082

Bushouse, H., Eisenhamer, J., Dencheva, N., et al. 2025, Zenodo, doi: 10.5281/zenodo.17515973

Byler, N., Dalcanton, J. J., Conroy, C., & Johnson, B. D. 2017, The Astrophysical Journal, 840, 44, doi: 10.3847/1538-4357/aa6c66

Cain, C., Lopez, G., D'Aloisio, A., et al. 2025, The Astrophysical Journal, 980, 83, doi: 10.3847/1538-4357/ada152

Cain, C., Smith, B., Bowling, G. B., et al. 2026, arXiv, doi: 10.48550/arXiv.2608.28745

Chabrier, G. 2003, Publications of the Astronomical Society of the Pacific, 115, 763, doi: 10.1086/376392

Charlot, S., & Fall, S. M. 2000, The Astrophysical Journal, 539, 718, doi: 10.1086/309250

Chen, C.-H., Ho, L. C., Li, R., & Inayoshi, K. 2025a, The Astrophysical Journal, 989, L12, doi: 10.3847/2041-8213/adee0a

Chen, C.-H., Ho, L. C., Li, R., & Zhuang, M.-Y. 2025b, The Astrophysical Journal, 983, 60, doi: 10.3847/1538-4357/ada93a

Chen, Z., Stark, D. P., Mason, C. A., et al. 2026a, The Astrophysical Journal, 1001, 236, doi: 10.3847/1538-4357/ae4220

Chen, Z., Stark, D. P., Mason, C. A., et al. 2026b, arXiv, doi: 10.48550/arXiv.2604.21516

Choustikov, N., Katz, H., Saxena, A., et al. 2024, Monthly Notices of the Royal Astronomical Society, 532, 2463, doi: 10.1093/mnras/stae1586

Christenson, H. M., Becker, G. D., D'Aloisio, A., et al. 2023, The Astrophysical Journal, 955, 138, doi: 10.3847/1538-4357/acf450

Conroy, C., Gunn, J. E., & White, M. 2009, The Astrophysical Journal, 699, 486, doi: 10.1088/0004-637X/699/1/486

Davis, K., Brooks, M., Simons, R. C., et al. 2026, arXiv, doi: 10.48550/arXiv.2606.00258

de Graaff, A., Hviding, R. E., Naidu, R. P., et al. 2025a, arXiv, doi: 10.48550/arXiv.2511.21820

de Graaff, A., Rix, H.-W., Naidu, R. P., et al. 2025b, Astronomy and Astrophysics, 701, A168, doi: 10.1051/0004-6361/202554681

Delvecchio, I., Daddi, E., Magnelli, B., et al. 2025, Astronomy and Astrophysics, 704, A313, doi: 10.1051/0004-6361/202557164

D'Eugenio, F., Cameron, A. J., Scholtz, J., et al. 2025, The Astrophysical Journal Supplement Series, 277, 4, doi: 10.3847/1538-4365/ada148

Ding, J., Yue, M., Zhu, Y., Fan, X., & Luo, Y. 2026, arXiv, doi: 10.48550/arXiv.2609.11879

Draine, B. T., & Li, A. 2007, The Astrophysical Journal, 657, 810, doi: 10.1086/511055

Eisenstein, D. J., Willott, C., Alberts, S., et al. 2023, arXiv. https://arxiv.org/abs/2306.02465

Geris, S., Maiolino, R., Ji, X., et al. 2026, arXiv, doi: 10.48550/arXiv.2606.21614
Greene, J. E., Labbe, I., Goulding, A. D., et al. 2024, The Astrophysical Journal, 964, 39, doi: 10.3847/1538-4357/ad1e5f
Greene, J. E., Setton, D. J., Furtak, L. J., et al. 2025, arXiv, doi: 10.48550/arXiv.2509.05434
Gronke, M., Dijkstra, M., McCourt, M., & Oh, S. P. 2017, Astronomy and Astrophysics, 607, A71, doi: 10.1051/0004-6361/201731013
Hainline, K. N., Maiolino, R., Juodžbalis, I., et al. 2025, The Astrophysical Journal, 979, 138, doi: 10.3847/1538-4357/ad9920
Hashemi, S., Becker, G. D., Zhu, Y., & Hong, H. 2025, Monthly Notices of the Royal Astronomical Society, 542, 104, doi: 10.1093/mnras/staf1225
Hayes, M. 2015, Publications of the Astronomical Society of Australia, 32, e027, doi: 10.1017/pasa.2015.25
Hayes, M. J., & Scarlata, C. 2023, The Astrophysical Journal, 954, L14, doi: 10.3847/2041-8213/acee6a
Inayoshi, K., & Maiolino, R. 2025, The Astrophysical Journal, 980, L27, doi: 10.3847/2041-8213/adaebd
Isobe, T., Feigelson, E. D., & Nelson, P. I. 1986, The Astrophysical Journal, 306, 490, doi: 10.1086/164359
Ivey, L. R., D'Eugenio, F., Maiolino, R., et al. 2026, arXiv, doi: 10.48550/arXiv.2604.09177
Jeon, J., Liu, B., Bromm, V., et al. 2025, arXiv, doi: 10.48550/arXiv.2508.14155
Ji, Z., Sun, Y., Giavalisco, M., et al. 2026a, arXiv, doi: 10.48550/arXiv.2606.09970
Ji, Z., Sun, Y., Giavalisco, M., et al. 2026b, The Astrophysical Journal Letters, 1008, L55, doi: 10.3847/2041-8213/ae9fea
Jiang, D., Jiang, L., Sun, S., Liu, W., & Fu, S. 2025, Nature Astronomy, 9, 1890, doi: 10.1038/s41550-025-02676-7
Johnson, B. D., Leja, J., Conroy, C., & Speagle, J. S. 2021, The Astrophysical Journal Supplement Series, 254, 22, doi: 10.3847/1538-4365/abef67
Johnson, B. D., Robertson, B. E., Eisenstein, D. J., et al. 2026, arXiv, doi: 10.48550/arXiv.2601.15954
Jones, B. L., Kocevski, D. D., Pacucci, F., et al. 2025, arXiv, doi: 10.48550/arXiv.2510.07376
Jones, G. C., Bunker, A. J., Saxena, A., et al. 2025, Monthly Notices of the Royal Astronomical Society, 536, 2355, doi: 10.1093/mnras/stae2670
Juodžbalis, I., Marconcini, C., D'Eugenio, F., et al. 2025, arXiv, doi: 10.48550/arXiv.2508.21748
Juodžbalis, I., Maiolino, R., Baker, W. M., et al. 2026, Monthly Notices of the Royal Astronomical Society, 546, stag086, doi: 10.1093/mnras/stag086
Kageura, Y., Ouchi, M., Yanagisawa, H., et al. 2026, arXiv, doi: 10.48550/arXiv.2608.14534
Kocevski, D. D., Finkelstein, S. L., Barro, G., et al. 2025, The Astrophysical Journal, 986, 126, doi: 10.3847/1538-4357/adbc7d
Kokorev, V., Caputi, K. I., Greene, J. E., et al. 2024, arXiv. https://arxiv.org/abs/2401.09981
Kokubo, M., & Harikane, Y. 2025, The Astrophysical Journal, 995, 24, doi: 10.3847/1538-4357/ae119e
Kriek, M., & Conroy, C. 2013, The Astrophysical Journal, 775, L16, doi: 10.1088/2041-8205/775/1/L16
Leja, J., Carnall, A. C., Johnson, B. D., Conroy, C., & Speagle, J. S. 2019, The Astrophysical Journal, 876, 3, doi: 10.3847/1538-4357/ab133c
Lin, X., Cai, Z., Wu, Y., et al. 2024, arXiv. https://arxiv.org/abs/2401.09532
Lin, X., Egami, E., Sun, F., et al. 2025, arXiv, doi: 10.48550/arXiv.2504.08028
Lin, X., Fan, X., Wang, F., et al. 2026a, The Astrophysical Journal, 996, 93, doi: 10.3847/1538-4357/ae1b9b
Lin, X., Fan, X., Cai, Z., et al. 2026b, The Astrophysical Journal, 997, 364, doi: 10.3847/1538-4357/ae2bdf
Lin, X., Fan, X., Cai, Z., et al. 2026c, arXiv, doi: 10.48550/arXiv.2605.21574
Liu, W., Veilleux, S., Rupke, D. S. N., et al. 2022, The Astrophysical Journal, 934, 160, doi: 10.3847/1538-4357/ac7a46
Ma, Y., Greene, J. E., Volonteri, M., et al. 2025, arXiv, doi: 10.48550/arXiv.2509.02662
Ma, Z., Egami, E., Zhu, Y., et al. 2026, arXiv, doi: 10.48550/arXiv.2601.15962
Madau, P., & Maiolino, R. 2026, arXiv, doi: 10.48550/arXiv.2602.22386
Maiolino, R., Risaliti, G., Signorini, M., et al. 2024, arXiv. https://arxiv.org/abs/2405.00504
Mascia, S., Matthee, J., Torralba, A., et al. 2026, arXiv, doi: 10.48550/arXiv.2608.25021
Mason, C. A., Treu, T., Dijkstra, M., et al. 2018, The Astrophysical Journal, 856, 2, doi: 10.3847/1538-4357/aab0a7
Mathews, E. P., Leja, J., Speagle, J. S., et al. 2023, The Astrophysical Journal, 954, 132, doi: 10.3847/1538-4357/ace720
Matthee, J., Naidu, R. P., Brammer, G., et al. 2024, The Astrophysical Journal, 963, 129, doi: 10.3847/1538-4357/ad2345
Matthee, J., Torralba, A., Pezzulli, G., et al. 2026, arXiv, doi: 10.48550/arXiv.2603.17667

McClymont, W., Tacchella, S., D'Eugenio, F., et al. 2025, Monthly Notices of the Royal Astronomical Society, 540, 190, doi: 10.1093/mnras/staf745

Naidu, R. P., Matthee, J., Oesch, P. A., et al. 2022, Monthly Notices of the Royal Astronomical Society, 510, 4582, doi: 10.1093/mnras/stab3601

Naidu, R. P., Matthee, J., Katz, H., et al. 2025, arXiv, doi: 10.48550/arXiv.2503.16596

Napolitano, L., Pentericci, L., Dickinson, M., et al. 2026, Astronomy and Astrophysics, 708, A102, doi: 10.1051/0004-6361/202556912

Obuchi, S., Ichikawa, K., Yamada, S., et al. 2026, The Astrophysical Journal, 997, 156, doi: 10.3847/1538-4357/ae1d6d

Osterbrock, D. E., & Ferland, G. J. 2006, Astrophysics of Gaseous Nebulae and Active Galactic Nuclei

Ouchi, M., Ono, Y., & Shibuya, T. 2020, Annual Review of Astronomy and Astrophysics, 58, 617, doi: 10.1146/annurev-astro-032620-021859

Pérez-González, P. G., Barro, G., Rieke, G. H., et al. 2024, The Astrophysical Journal, 968, 4, doi: 10.3847/1538-4357/ad38bb

Pérez-González, P. G., Barro, G., Carniani, S., et al. 2026, arXiv, doi: 10.48550/arXiv.2602.20247

Planck Collaboration, Aghanim, N., Akrami, Y., et al. 2020, Astronomy and Astrophysics, 641, A6, doi: 10.1051/0004-6361/201833910

Rinaldi, P., Pérez-González, P. G., Rieke, G. H., et al. 2025a, The Astrophysical Journal, 994, 86, doi: 10.3847/1538-4357/ae089c

Rinaldi, P., Rieke, G. H., Wu, Z., et al. 2025b, arXiv, doi: 10.48550/arXiv.2507.17738

Rinaldi, P., Bonaventura, N., Rieke, G. H., et al. 2025c, The Astrophysical Journal, 992, 71, doi: 10.3847/1538-4357/adfa10

Robertson, B. E., Johnson, B. D., Tacchella, S., et al. 2026, arXiv, doi: 10.48550/arXiv.2601.15956

Scarlata, C., Hayes, M., Panagia, N., et al. 2024, arXiv, doi: 10.48550/arXiv.2404.09015

Scholtz, J., Carniani, S., Parlanti, E., et al. 2025, arXiv, doi: 10.48550/arXiv.2510.01034

Shields, J. C., & Ferland, G. J. 1993, The Astrophysical Journal, 402, 425, doi: 10.1086/172147

Singha, M., Malhotra, S., & Rhoads, J. E. 2025, arXiv, doi: 10.48550/arXiv.2510.26990

Sok, V., Nelson, E. J., Begelman, M. C., et al. 2026, arXiv, doi: 10.48550/arXiv.2606.23778

Tang, M., Stark, D. P., Topping, M. W., Mason, C., & Ellis, R. S. 2024a, The Astrophysical Journal, 975, 208, doi: 10.3847/1538-4357/ad7eb7

Tang, M., Stark, D. P., Ellis, R. S., et al. 2024b, Monthly Notices of the Royal Astronomical Society, 531, 2701, doi: 10.1093/mnras/stae1338

Tang, M., Stark, D. P., Mason, C. A., et al. 2026, arXiv, doi: 10.48550/arXiv.2604.03563

Torralba, A., Matthee, J., Pezzulli, G., et al. 2026, Astronomy and Astrophysics, 705, A147, doi: 10.1051/0004-6361/202555596

Wang, B., Leja, J., Katz, H., et al. 2025, arXiv

Wang, B., Leja, J., Labbe, I., et al. 2026, arXiv, doi: 10.48550/arXiv.2602.06024

Williams, C. C., Alberts, S., Ji, Z., et al. 2024, The Astrophysical Journal, 968, 34, doi: 10.3847/1538-4357/ad3f17

Yanagisawa, H., Ouchi, M., Kiyota, T., et al. 2026, arXiv, doi: 10.48550/arXiv.2606.09726

Yue, M., Eilers, A.-C., Ananna, T. T., et al. 2024, doi: 10.48550/arXiv.2404.13290

Zhang, J., Egami, E., Sun, F., et al. 2026, The Astrophysical Journal, 997, 250, doi: 10.3847/1538-4357/ae2681

Zhong, Y., Chen, X., Ichikawa, K., et al. 2026, arXiv, doi: 10.48550/arXiv.2603.13736

Zhu, Y., Bonaventura, N., Sun, Y., et al. 2026a, The Astrophysical Journal, 997, 301, doi: 10.3847/1538-4357/ae29b4

Zhu, Y., Fan, X., Keating, L. C., et al. 2026b, arXiv, doi: 10.48550/arXiv.2608.19311